AGU ADVANCING EARTH AND SPACE SCIENCES

JGR Oceans

RESEARCH ARTICLE
10.1029/2025JC023561

The North Atlantic Subpolar Gyre and Phytoplankton Bloom Under Potential Future Climate Scenarios

Sophy Oliver[1], Andrew Yool[1], Lee de Mora[2], Stephen Kelly[1], Spencer K. Liddicoat[3], Alexandra Loveridge[1], Robin S. Smith[4], and Ekaterina Popova[1]

[1]National Oceanography Centre, Southampton, UK, [2]Plymouth Marine Laboratory, Plymouth, UK, [3]Met Office Hadley Centre, Exeter, UK, [4]National Centre for Atmospheric Science, University of Reading, Reading, UK

Key Points:

- Studies indicate the North Atlantic subpolar gyre (SPG) convection and phytoplankton bloom (NAB) are projected to undergo abrupt decline
- We use idealized emissions scenarios and an Earth system model to evaluate the conditions for decline and recovery of the SPG and NAB
- Zero carbon emissions do not allow NAB recovery beyond 1.5–2°C, and recovery from 1.5–2°C takes at least several centuries

Supporting Information:

Supporting Information may be found in the online version of this article.

Correspondence to:

S. Oliver,
sophy.oliver@noc.ac.uk

Citation:

Oliver, S., Yool, A., de Mora, L., Kelly, S., Liddicoat, S. K., Loveridge, A., et al. (2026). The North Atlantic subpolar gyre and phytoplankton bloom under potential future climate scenarios. *Journal of Geophysical Research: Oceans*, *131*, e2025JC023561. https://doi.org/10.1029/2025JC023561

Received 6 OCT 2025
Accepted 2 JUL 2026

Author Contributions:

Conceptualization: Sophy Oliver, Andrew Yool, Ekaterina Popova
Data curation: Sophy Oliver, Andrew Yool
Formal analysis: Sophy Oliver
Funding acquisition: Ekaterina Popova
Investigation: Sophy Oliver
Methodology: Sophy Oliver, Andrew Yool, Lee de Mora, Stephen Kelly, Ekaterina Popova
Software: Spencer K. Liddicoat, Robin S. Smith

Abstract The North Atlantic phytoplankton bloom (NAB) forms the base of the food web upon which marine ecosystem services throughout the northern North Atlantic rely. The NAB's nutrient supply is predominantly driven by deep winter mixing, which is most pronounced in the subpolar gyre where it has been projected to abruptly decline within the next few decades. Here we use idealized experiments with an Earth system model to investigate how mixed layer depth, surface nutrients and chlorophyll concentrations over the gyre may respond to positive carbon emissions followed by both zero and negative emissions mitigation efforts initiated at various Global Warming Levels (GWLs). Results show a decline in all three variables during positive emissions, with the warmer the GWL the less likely the prospect of recovery back to pre-industrial conditions. In the scenario where carbon emissions are held at zero once reaching a GWL of 1.5°C, the NAB started to recover toward preindustrial conditions. However, zero emissions after 2.5°C and warmer showed a continued decline in the NAB. These results suggest a tipping threshold may lie between 1.5 and 2.5°C GWL, beyond which only negative emissions can achieve recovery of the NAB. Even in the lowest warming scenario examined, 1.5°C, recovery of the NAB did not occur within 5 centuries under zero emissions, nor did it occur within one century under negative emissions.

Plain Language Summary The North Atlantic Ocean has an annual spring bloom of microscopic algae that supports its marine ecosystems. This bloom occurs because winter mixing brings up nutrients from the deep ocean, particularly in the subpolar gyre. With global warming, research indicates mixing in the gyre will rapidly decline in the next few decades. Here we use computer simulations of the Earth system to project the future under possible carbon dioxide (CO_2) emission scenarios. These scenarios begin by adding CO_2 to the atmosphere (positive emissions) until reaching a certain level of global warming, followed either by a period of no additional CO_2 (zero emissions) or CO_2 removal (negative emissions). We find that under continued positive emissions the bloom gets progressively smaller. Switching to zero emissions before exceeding 1.5–2°C of global warming allows the bloom to recover, but it takes more than 5 centuries to return to pre-industrial conditions. Once 1.5–2°C of global warming is exceeded then switching to zero emissions is insufficient to reverse the decline of the bloom. Negative emissions using some future technologies could potentially restore the bloom from as much as 5°C of global warming, but such recovery timescales would be far beyond human lifetimes and policy timescales.

1. Introduction

Deep winter mixing in the ocean is vital for the supply of nutrients from the ocean's interior to its surface waters. This drives the productivity of marine phytoplankton which bloom when light availability increases in the spring. The North Atlantic Bloom (NAB) is most pronounced in the Atlantic's subpolar gyre (SPG), a large-scale cyclonic gyre with deep winter mixing located between 45°N and 65°N within the Labrador and Irminger Seas (Biri & Klein, 2019). The NAB initiates in May in the SPG region and expands across most of the North Atlantic over the following months (Henson et al., 2009). The NAB forms the base of the food web upon which many higher trophic levels depend, including herring, mackerel, cod and tuna (Moyano et al., 2022; Pershing & Stamieszkin, 2020). For example, the copepod (zooplankton) species *Calanus finmarchicus* has multiple life stages timed according to the seasonality of the NAB (Jacobsen et al., 2022; Mayor et al., 2020), which are then preyed upon by first feeding cod larvae (Pershing & Stamieszkin, 2020). It is clear that the NAB plays an important role in the supply of stock for fisheries within the North Atlantic.

Supervision: Andrew Yool, Ekaterina Popova
Validation: Sophy Oliver, Stephen Kelly
Visualization: Sophy Oliver, Alexandra Loveridge
Writing – original draft: Sophy Oliver
Writing – review & editing: Sophy Oliver, Andrew Yool, Lee de Mora, Stephen Kelly, Spencer K. Liddicoat, Alexandra Loveridge, Robin S. Smith, Ekaterina Popova

The SPG has been identified as having a potential tipping point, defined previously as a critical threshold in some gradual forcing at which a small additional amount of forcing results in a nonlinear abrupt shift in the system (Armstrong McKay et al., 2022; Brovkin et al., 2021; Thomas, 2016). Increased stratification caused by warming and/or freshening may cause the SPG to "collapse", whereby the gyre circulation is greatly weakened, and deep winter mixing is largely reduced (Arellano-Nava et al., 2022; Kwiatkowski et al., 2020; Sgubin et al., 2017; Swingedouw et al., 2020, 2021). There have been observed abrupt shifts in the SPG in the past, such as prior to the Little Ice Age in the 13th century (Arellano-Nava et al., 2022; Jalali et al., 2019) and more recently in the mid-1990s (Born et al., 2015).

Studies have shown that some models project abrupt change in the SPG within the next few decades (Gu et al., 2024; Hieronymus et al., 2024; Kelly et al., 2025; Menary et al., 2025; Sgubin et al., 2017; Swingedouw et al., 2021; Terpstra et al., 2025). However, the majority of models do not project such an abrupt change, with only 4/35 (Swingedouw et al., 2021)—24/57 (Terpstra et al., 2025) of Coupled Model Intercomparison Project Phase 6 (CMIP6) models and 7/40 of CMIP5 models (Sgubin et al., 2017) projecting abrupt change in the SPG. Whether a collapse is projected is highly dependent on the definition of "collapse" in each study, and which environmental variables are analyzed. Swingedouw et al. (2021) and Sgubin et al. (2017) searched for an abrupt cooling in sea surface temperature, while Kelly et al. (2025) searched for an abrupt shoaling of the mixed layer depth (MLD) and Terpstra et al. (2025) searched for an abrupt shift in either sea surface salinity, MLD, sea surface temperature or surface air temperature. As Terpstra et al. (2025) were more inclusive in their definition of abrupt change within the SPG, their result of 40% of CMIP6 models projecting abrupt change in the SPG may be more informative, most such events occurring within 0.3–3°C of mean global warming. For context, in 2024 the observed 10-year mean global warming reached approximately 1.3°C (Tollefson, 2025) and it is projected to reach 1.5°C by 2030 and 3°C by the end of the century under current policies (e.g., Wyser et al., 2020).

A collapse in SPG deep winter mixing and convection may lead to both a localized effect on climate in the North Atlantic and neighboring continents (Arellano-Nava et al., 2022; Armstrong McKay et al., 2022; Swingedouw et al., 2020, 2021) and more wide-reaching consequences (Armstrong McKay et al., 2022). Regarding the NAB, a SPG convection collapse is projected to cause a decrease in surface nutrients (Lavoie et al., 2017; Sein et al., 2020), resulting in changes to both the NAB's magnitude (Fu et al., 2016; Kwiatkowski et al., 2020; Nakamura & Oka, 2019; Yool et al., 2015) and its phenology (Asch et al., 2019; Henson et al., 2013, 2017; Sein et al., 2020; Yamaguchi et al., 2022). Plankton community composition may also be impacted, with a reduction in diatom and coccolithophores and a shift towards smaller phytoplankton (Bopp et al., 2005; Fu et al., 2016; Grieve et al., 2017; Jensen et al., 2017). These changes in the NAB will have consequences for the efficiency of the biological carbon pump and long term carbon drawdown and storage (Boot et al., 2023; Bopp et al., 2005; Cabrera-Brufau et al., 2021), and will influence higher trophic levels within the North Atlantic, from zooplankton to fish (Boot et al., 2025; Jacobsen et al., 2022; Moyano et al., 2022; Pershing & Stamieszkin, 2020). How long these impacts will last depends on how long the SPG takes to recover to a state that can support a strong NAB, if it recovers at all. The SPG was modelled to recover from two separate collapses during the Holocene within 30–40 years (Klus et al., 2018), therefore impacts may be likely to be short-lived. However, with continued anthropogenic global warming, a future collapsed SPG may only recover if and when warming is stabilized or reversed, if recovery is indeed possible.

In this study we use the United Kingdom Earth System Model v1.2 (UKESM) to project how the SPG convection and the NAB may respond to global warming reaching different global warming levels (GWLs), attempts to stabilize warming via zero carbon emissions, and warming being reduced using carbon dioxide removal techniques. More specifically, as UKESM projects abrupt shifts in the SPG from the year 2040 (Kelly et al., 2025), we aim to understand under what climate mitigation conditions this shift is reversible, if at all. A greater understanding of the long-lasting repercussions of different GWLs reached and their potential impacts will allow decision makers to understand the consequences of each degree of global warming and may lead to further prioritization of climate mitigation efforts.

2. Methodology

2.1. UKESM1.2

We use the Earth system model UKESM1.2 (Mulcahy et al., 2023; Sellar et al., 2019), earlier versions of which have contributed to CMIP6. UKESM's core physical climate model is the Hadley Center Global Environment

Model version 3 Global Coupled (GC) version 3.1 configuration, HadGEM3-GC3.1 (Kuhlbrodt et al., 2018; Williams et al., 2018). This is augmented in the atmosphere with interactive stratospheric-tropospheric trace gas chemistry, on the land with terrestrial biogeochemistry and ecosystem dynamics, and in the ocean with marine biogeochemistry. UKESM1.2 is extended from UKESM1.1 (Mulcahy et al., 2023) by the inclusion of dynamic Greenland and Antarctica ice sheet components (UniCiCles; Smith et al., 2021).

Within UKESM's ocean, component models represent physics and general circulation (NEMO; Madec et al., 2023; Storkey et al., 2018), sea ice (CICE; Ridley et al., 2018) and marine biogeochemistry (MEDUSA; Yool et al., 2013). MEDUSA is a medium-complexity model, including cycles of nitrogen, silicon, iron, dissolved oxygen, carbon and alkalinity, and two size classes of both phytoplankton and zooplankton. The ocean is resolved at approximately 1° resolution with 75 depth levels. UKESM's ocean performance is evaluated in Yool et al. (2021).

UKESM is run here in CO_2 emissions-driven mode, whereby atmospheric CO_2 concentration is interactive rather than fixed and varies according to fluxes passing between the atmosphere, land and ocean. This allows the investigation of idealized runs varying in anthropogenic addition (positive emissions) and removal (negative emissions) of CO_2 to drive different levels of global warming, such as was done by Smith et al. (2026) to understand ice sheet, sea-ice and sea level responses.

2.2. Experiment Design

We analyze 15 idealized model runs as in the TIPMIP ESM protocol (Winkelmann et al., 2025), shown in Figures 1a–1c and fully named in Table S1 in Supporting Information S1. The pre-industrial simulation spans more than 600 years with zero emissions and has an atmospheric carbon dioxide concentration of approximately 280 ppm. The constant positive emissions simulation branches off from the pre-industrial by adding 8 PgC per year (approximately +0.2°C of global warming per decade) until the running for more than 350 years and exceeding 6°C of global warming. The positive emissions experiment is idealized and does not attempt to represent realistic historical emissions. However, it has been designed so that years 10–50 of the positive emissions simulation align approximately with the Historical time period 1975–2015. Over these 40 years both the rate of global warming (approximately +0.2°C per decade) and increase in atmospheric CO_2 concentrations (approximately +17 ppm per decade) compare well to observations.

From thepositive emissions simulation, 7 different zero emissions runs branch off at the global warming levels (GWLs) 1.5, 2, 2.5, 3, 4, 5 and 6°C. After 50 years of stabilization in each respective warming scenario (except 2.5°C), a negative emissions simulation branches off. In each negative emissions simulation 4 PgC/yr is removed from the atmosphere, mimicking a hypothetical scenario where there are successful and significant technique(s) for removing carbon dioxide directly from the atmosphere. The negative emissions experiments are truncated during post-processing to end when the amount of cumulative emissions return to zero, which is the case for the 1.5, 2 and 3°C runs. Figures 1a–1c show the cumulative emissions, atmospheric CO_2 concentration and global mean surface air temperature (GMSAT) anomaly relative to the mean of the pre-industrial for each of these 15 runs.

2.3. Subpolar Gyre and North Atlantic Bloom Metrics

To best display the change in the SPG and NAB over the experiments, a SPG region is defined, as well as three key physical and biogeochemical variables. The SPG region (Figure 1j) is chosen using a sea surface height (SSH) contour, similar to Foukal and Lozier (2017), but bounded by the tighter −1.05 m SSH contour, as shown in Figure S1 in Supporting Information S1 (and overlain on all spatial maps included in the results). The −1.05 m contour is first calculated from annual minima of monthly averages, then taken as the mean over the entire pre-industrial simulation. The region remains spatially fixed throughout the study. The focus of this study is the SPG mixing-driven supply of nutrients and associated NAB, therefore this contour is chosen as it tightly encloses the area of deep winter mixing in the SPG (see Figure S2d in Supporting Information S1).

The main focus of this study is the NAB, and how changes in the SPG and SPG-associated nutrient supply influence the NAB. Therefore the key variable chosen to examine SPG convection is annual maximum mixed layer depth (MLD; m), calculated as the depth at which density exceeds the density at the surface by >0.03 kg m^{-3}. The key variables chosen to indicate the strength of the NAB are annual maximum surface dissolved inorganic

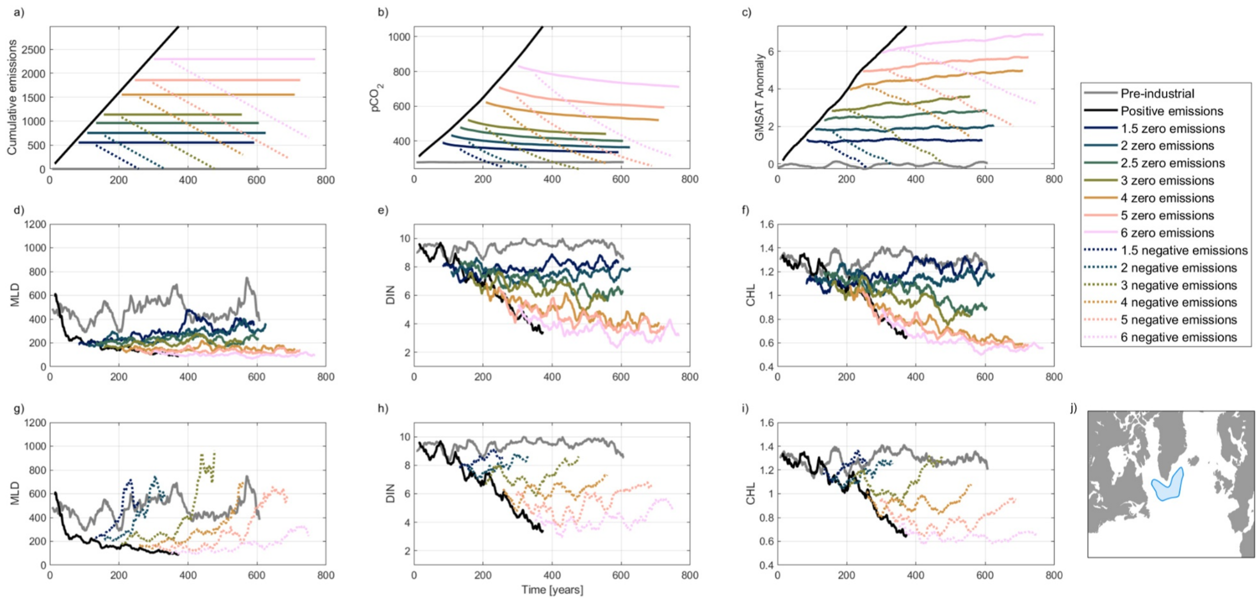

Figure 1. 30-year running mean for selected variables during all UKESM experiments, regionally averaged over the (a–c) globe or (d–i) subpolar gyre (SPG) region. The location of the SPG region is shown in the bottom-right panel (j). The running mean is calculated as the average over 15 years prior to and after each year. Variables plotted are (a) cumulative emissions [PgC], (b) atmospheric pCO_2 [ppm], (c) global mean surface air temperature (GMSAT) anomaly [°C], (d, g) mixed layer depth (MLD) [m], (e, h) surface dissolved inorganic nitrogen (DIN) [mmol N m^{-3}] and (f, i) surface chlorophyll concentration (CHL) [mg Chl m^{-3}]. The experiments shown are the pre-industrial (gray solid line), positive emissions (black solid line), and the zero emissions (colored solid lines) and negative emissions (colored dashed lines) for various global warming levels.

nitrogen (DIN; mmol N m^{-3}) and surface chlorophyll-a concentration in both non-diatoms and diatoms combined (CHL; mg Chl m^{-3}). These are calculated from monthly means, of which the annual maxima are taken and then, if required, the area-weighted regional average over the SPG region. These key variables are consistent with those analyzed by Kelly et al. (2025) who determined SPG and NAB collapse in UKESM, therefore we provide a consistent methodology when continuing their approach to include SPG and NAB recovery.

We acknowledge two of these three metrics are difficult to compare with observations as they must be measured in-situ, and choosing metrics that can be observed with greater spatial and temporal coverage, such as SSH, might seem preferable. However, a comparison of SSH and MLD in our model experiments (see Figure S3 in Supporting Information S1) suggests that SSH is not a suitable proxy to indicate changes in MLD, and hence would not provide a good indication of mixing-driven nutrient supply to the NAB.

2.4. Model Validation

As previously mentioned, the positive emissions simulation is an idealized experiment that does not precisely represent the historical record, but has a similar rate of emissions and warming as that of the second half of the 20th century. This allows a comparison of part of the positive emissions simulation to both observations (CMEMS, 2023; de Boyer Montégut, 2023; de Boyer Montégut et al., 2004; Garcia et al., 2018; Gohin et al., 2010) and to the modelled Historical period by UKESM, as shown in Figure S2 in Supporting Information S1. The spatial distribution of annual maximum mixed layer depth (MLD), surface dissolved nitrogen (DIN) and surface chlorophyll (CHL) modelled by UKESM over the Historical period are comparable to observations. Features captured are the high mixing, nutrients and chlorophyll in the SPG and off the east coast of Greenland. As general spatial patterns are correctly represented by UKESM, we can with confidence use UKESM for the idealized experiments carried out in this study to provide a projection of how the ocean may respond to different future global warming scenarios. Nonetheless, the model does display biases which have been previously described (Mulcahy et al., 2023; Sellar et al., 2019; Yool et al., 2021).

The Historical period modelled by UKESM also compares well with the early section of the positive emissions simulation and therefore can provide context when considering how the idealized positive emissions run relates to reality. The main difference is a slight reduction in MLD, DIN and CHL over the North Atlantic. This may be because the positive emissions simulation experiences more global warming than the Historical period during the first 25 years (results not shown), causing a greater reduction in SPG MLD and hence also in nutrients and phytoplankton.

2.5. Definition of "Recovery"

This study does not seek to identify a moment of collapse within the continuous decline of the SPG and NAB metrics, as this was extensively covered by Kelly et al. (2025). Instead, we focus on whether the system can recover from this decline. The SPG convection is deemed to be recovered once the 30-year running average MLD reaches or exceeds the mean of the pre-industrial, and the NAB recovered once the same happens to both DIN and CHL. If the model experiment is not run long enough for this to be reached then a projected recovery is calculated as follows; (a) using linear regression calculate the trend of every 30-year segment of the run, (b) average these trends to yield one mean trend (m) over the whole model run, (c) define the starting point ($y0$) as the average of the first 30 years, (d) calculate the time (T) required to exceed the mean of the pre-industrial ($y\text{End}$) as $T = (y\text{End} - y0)/m$. There are uncertainties in the projected recovery timescales associated with the choice of method to calculate the trends. These are explored in Section 4.3.

3. Results

3.1. Positive Emissions

During the positive emissions simulation there is a rapid shoaling of MLD and a large reduction in surface DIN and CHL. When averaged over the SPG region, the 30-year running means (i.e., averaged over 15 years either side of each year) over the positive emissions simulation show a rapid decline in MLD from the start, and an overall decline in both DIN and CHL from approximately 80 years (Figure 1, subplots g-i, black lines). Table 1 and Figures S4–S6 in Supporting Information S1 show the mean of the trends in the SPG regional average of MLD, DIN and CHL over the positive emissions simulation, calculated using linear regression for every 30-year segment throughout the run. Positive emissions cause a trend of −15 m of MLD per decade, −170 μmol N m^{-3} of DIN per decade, and −18 μg Chl m^{-3} per decade in the SPG. After 135 years of positive emissions (which approximately aligns with the year 2100 and a GWL of 2.5–3°C), the 30-year running means for MLD, DIN and CHL over the SPG are reduced to 32%, 74%, and 84% of the pre-industrial mean, respectively.

Spatial distributions of the trends in Figure 2 show variation both within the SPG and within the wider region surrounding the SPG. The trend in MLD reduction is strongest in the SPG, while contrastingly there is a deepening in mixing off the eastern coast of Greenland (Figure 2a). There are negative trends in both DIN and CHL in the Labrador Sea (the west side of our defined SPG region) but this is not as strongly negative in the Irminger Sea (the east side), and there is a negative trend around Iceland and the UK (Figures 2b and 2c).

3.2. Zero Emissions

3.2.1. Regionally Averaged SPG Trends

Figures 1d–1f show the response in the SPG MLD, DIN and CHL over the zero emissions experiments, where the cessation of carbon emissions occurred at 7 different GWLs ranging from 1.5°C to 6°C. As to be expected, the warmer the scenario, the shallower the MLD and lower the surface nutrients and chlorophyll. In outline, the zero emissions experiments fall into three groups: those in which both the SPG and NAB recover (1.5 and 2°C GWLs), those in which the SPG recovers but the NAB does not (2.5 and 3°C GWLs), and those in which neither the SPG nor the NAB recover (4, 5 and 6°C GWLs).

The zero emissions experiments at 1.5 and 2°C GWLs display a positive trend in all three variables, with an increase of 3 m decade^{-1} in MLD, 3–8 μmol N m^{-3} decade^{-1} of DIN, and 0.32–3 μg Chl m^{-3} decade^{-1} of CHL (see Table 1). If extrapolated, these trends indicate that, with enough time, the weakened SPG and NAB will eventually recover back to pre-industrial conditions if zero emissions are achieved by these GWLs. 2°C is the warmest GWL to achieve eventual recovery of the NAB under zero emissions.

The zero emissions experiments at 2.5 and 3°C GWLs display a slightly positive trend in MLD, with an increase of 0.7–1 m decade^{-1}. Therefore, 3°C is the warmest GWL to achieve an eventual recovery of the SPG under zero emissions, at least when using MLD as a metric for the state of the SPG. However, these experiments continue to

Table 1
Regionally Averaged Results Over the Subpolar Gyre for the Pre-Industrial (PI), Positive Emissions (PE), Zero Emissions (ZE) and Negative Emissions (NE) Experiments

	Trend Δ/Decade			Recovery period [yrs]		
	MLD [m]	DIN [μmol N m^{-3}]	CHL [μg Chl m^{-3}]	MLD	DIN	CHL
PI	−0.99	−0.79	−0.85			
PE	−15	−170	−18			
1.5°C ZE	3.1	3	3	911(329)	4,521	628(323)
2°C ZE	3	8	0.32	929	2176	3,838
2.5°C ZE	0.7	−42	−6.2	3,879		
3°C ZE	1.1	−46	−7.1	2861		
4°C ZE	−0.061	−52	−9.3			
5°C ZE	−0.12	−55	−9.1			
6°C ZE	−0.62	−43	−6.9			
1.5°C NE	23	28	4.2	107(91)	552	287(95)
2°C NE	20	0.56	5.7	122(139)	27,037[a]	298
2.5°C NE	–	–	–	–	–	–
3°C NE	22	54	6.6	134(222)	497	321(244)
4°C NE	21	53	5.2	148(292)	586	532
5°C NE	10	13	0.12	312(312)	2632	29,749
6°C NE	3.3	9.3	−2.5	1,124	5,627	

Note. Columns 2–4 show the trend (calculated as a mean linear regression of all 30-year periods) in mixed layer depth (MLD) [m per decade], surface dissolved inorganic nitrogen (DIN) [μmol N m^{-3} per decade] and surface chlorophyll concentration (CHL) [μg Chl m^{-3} per decade], respectively. Columns 5–7 show the extrapolated (modelled) number of years to recover back to pre-industrial levels. See Section 2.5 for further detail on the calculation of trends and recovery periods. [a]This anomaly is discussed in Section 4.3.

have a negative trend in both DIN and CHL, with decreases of 42–46 μmol N m^{-3} decade^{-1} and 6.2–7.1 μg Chl m^{-3} decade^{-1}, respectively. Therefore, at these GWLs, even if the SPG recovers, the NAB instead continues to decline.

The zero emissions experiments at 4, 5, and 6°C GWLs display a negative trend in all three variables, with decreases of 0.061–0.62 m decade^{-1} in MLD, 43–55 μmol N m^{-3} decade^{-1} of DIN, and 6.9–9.3 μg Chl

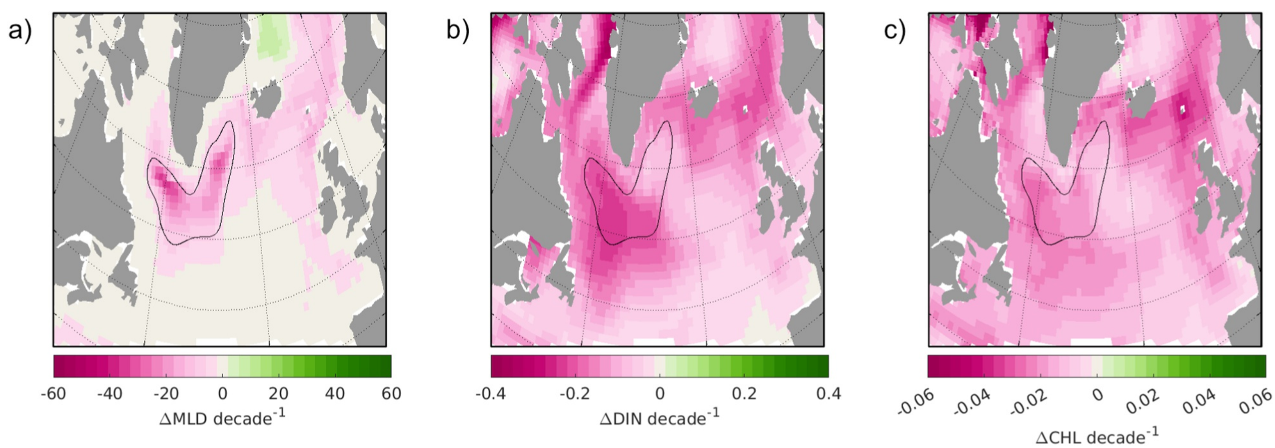

Figure 2. North Atlantic spatial distribution of the mean trend over the positive emissions experiment for (a) mixed layer depth (MLD) [m per decade], (b) surface dissolved inorganic nitrogen (DIN) [mmol N m^{-3} per decade] and (c) surface chlorophyll concentration (CHL) [mg Chl m^{-3} per decade]. The defined subpolar gyre region is overlain (black solid line). Spatial maps in this study were plotted using the MATLAB package "M_Map" (Pawlowicz, 2005).

m^{-3} $decade^{-1}$ of CHL. This suggests that, even if zero emissions were achieved warmer than 3°C of global warming, neither the SPG or the NAB will ever recover and instead will continue to decline under zero emissions.

3.2.2. Spatial Variability

The preceding analysis describes the trends in MLD, DIN and CHL averaged over the defined SPG region. However, there is substantial spatial variation in these trends both within the SPG and across the wider North Atlantic (see Figures 3c and 4 and Figure S7 in Supporting Information S1). Figures 4a–4f show that while the zero emissions experiments at 1.5 and 2°C GWLs display a positive trend in all three variables within the Labrador Sea, there is a negative trend in DIN and CHL in the neighboring Irminger Sea even at the 1.5°C GWL. To help show the difference between these sub-regions within the gyre, sub-regional averages are provided in Figures S8–S9 in Supporting Information S1 for both the western and eastern side of the SPG, divided by the longitude 42°W. Despite this difference in trends between the western and eastern side of the gyre shown by Figure 4, by the end of the 1.5 and 2°C zero emissions simulations their DIN and CHL concentrations are comparable (see Figures S8e–S8f and S9e–S9f in Supporting Information S1). This is because DIN and CHL do not decline as much in the eastern side of the gyre under positive emissions.

Somewhat surprisingly, MLD shows the opposite story in the Irminger Sea. The greatest positive trend in MLD within the SPG over the 2–5°C zero emissions experiments occurs in the Irminger Sea (e.g., Figure S7d in Supporting Information S1), yet this does not cause a positive trend in DIN and CHL in the same location (e.g., Figures S7e–S7f in Supporting Information S1).

3.3. Negative Emissions

3.3.1. Regionally Averaged SPG Trends

Figures 1g–1i show the response of MLD, DIN and CHL in the SPG region over the negative emissions experiments initialized from a range of GWLs between 1.5° and 6°C. All three variables show an overall positive trend in every scenario (excluding CHL in the 6°C experiment in Figure 1i). Therefore, extrapolation indicates the SPG and NAB will eventually recover back to pre-industrial conditions if negative emissions are achieved prior to warming beyond 5°C. In general, the warmer the scenario reached, the weaker the positive trends in MLD, DIN and CHL during negative emissions, as shown in Table 1. Interestingly, MLD overshoots and exceeds the pre-industrial mean MLD in several negative emissions experiments (see Figure 1g). Potential reasons for this are discussed in Section 4.2.

3.3.2. Spatial Variability

Figure 3c, Figures S10 and S11 in Supporting Information S1 show the spatial variation in the MLD, DIN and CHL trends within the North Atlantic over the negative emissions experiments. While there is generally a positive trend in these three metrics throughout the North Atlantic, the Irminger Sea in particular shows a consistent negative trend in DIN and CHL for all of the negative emissions experiments. Sub-regional averages over the western and eastern side of the gyre for these simulations are shown in Figures 8g–8i and Figures S9g–S9i in Supporting Information S1. They also show that recovery under negative emissions is more clear in the western side of the gyre.

3.4. The Recovered State

Zero emissions achieved above 2°C GWL do not initiate the recovery of the NAB. Even where zero emissions are achieved by 1.5 or 2°C GWL, extrapolating the trends in DIN and CHL finds that the NAB may only recover after centennial to millennial timescales (see Table 1 and Figure 3b). Meanwhile, if negative emissions can be achieved by 5°C GWL the NAB will eventually recover, but the extrapolated trends indicate recovery will take at least 100 years even starting from the best case scenario of 1.5°C maximum global warming. As these results are influenced by the choice of method to calculate trends, see Section 4.3 for an alternative method to understand associated uncertainty.

Even if the SPG regionally averaged MLD, DIN and CHL recover to pre-industrial levels, the question remains as to whether the spatial patterns also return to as they were during the pre-industrial. Here we have used the positive emissions experiment plus the 3°C GWL scenarios to answer this question, as 3°C is the warmest negative emissions scenario run long enough to return to zero cumulative emissions. Spatial distributions of MLD, DIN

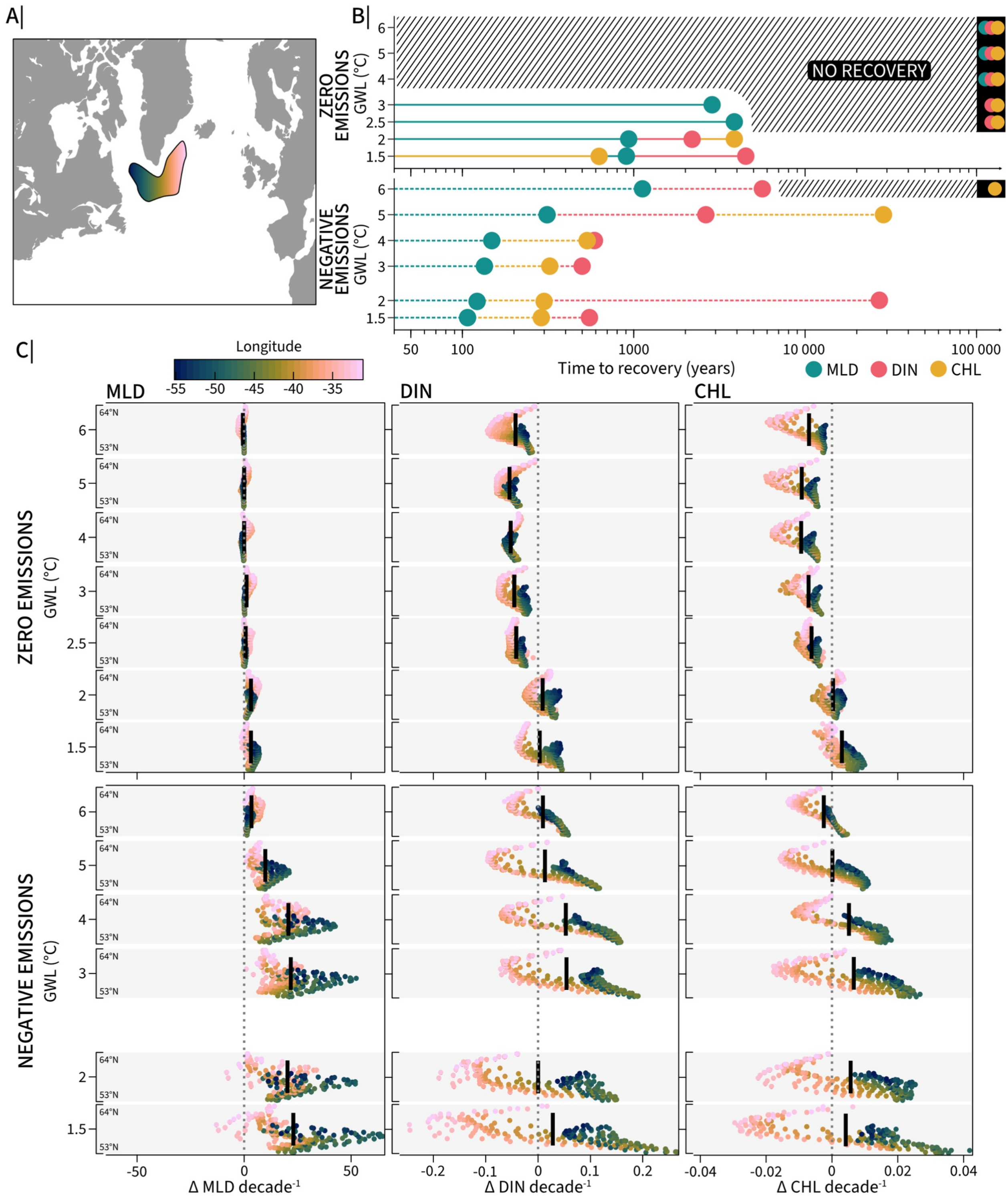

Figure 3. Summary of trends and recovery times averaged over and within the subpolar gyre (SPG) region. (a) Map showing the SPG region, defined using the sea surface height contour −1.05 m. (b) The time required for the SPG (according to mixed layer depth (MLD); green dots) and the North Atlantic bloom (according to surface nitrate (DIN) and chlorophyll (CHL); red dots and yellow dots, respectively) to recover to pre-industrial levels after achieving (top panel of b) zero emissions and (bottom panel of b) negative emissions once reaching various global warming levels (GWLs). The shaded region and the black boxes on the right of (b) show the zone of no recovery, that is the GWLs where at least one metric never recovers. (c) The trend in MLD, DIN and CHL over the (top panel of c) zero emissions and (bottom panel of c) negative emissions runs. The horizontal black lines show the SPG regional mean trend and the individual colored dots show the trend for each grid point within the SPG region, colored according to longitude and vertically spread along sections of the *y*-axis according to latitude. Negative trends indicate a metric will never recover and positive trends indicate it will eventually recover.

and CHL are shown in Figure 5, Figures S12 and S13 in Supporting Information S1, respectively, for the start of the positive emissions and 3°C GWL zero emissions experiments, and for the end of the 3°C GWL negative emissions experiment. The same regions which experience a loss of mixing, nitrate and chlorophyll after 3°C of global warming also experience a gain in these variables after over 300 years of negative emissions. Therefore, after negative emissions the regions of high mixing shown in Figure 5c return in the same locations as they were at the start of the positive emissions in Figure 5a, as do both nitrate and chlorophyll shown in Figures S12 and S13 in Supporting Information S1, respectively.

This return toward the pre-industrial state is also shown in depth space in Figure 6, which displays the water column averaged over the SPG region, shown as the difference to the pre-industrial. During the positive emissions experiment the MLD shoals as the water column becomes more stratified, leading to less upwelling of nutrients into the surface and an increase in nutrients at depth. The non-diatoms respond to the reduced nutrients at the surface by moving down to the base of the mixed layer, while diatoms are more greatly impacted and show only a large decline in the surface. Then, during the negative emission experiment, the MLD deepens as the water column becomes less stratified again. Nutrients and diatoms return to the surface, although not as prominently as before the positive emissions.

These results indicate that both the SPG and NAB can recover to a similar state to the pre-industrial after a significant decline. We use the term "similar state" here, as there are still differences between the pre-industrial and the end of the 3°C negative emissions run, particularly in the sub-surface nutrients. After the initial increase in sub-surface nutrients under positive emissions, there is then a long-term decrease in sub-surface nutrients which do not show signs of reversal under negative emissions (Figures 6b and 6c). This long-term decrease in sub-surface nutrients corresponds with an accumulation of nutrients at approximately 2,000 m (not shown). The particular difficulty to recover nitrate is also highlighted by the recovery timescales (see Table 1 and Figure 3b), which show that of the three metrics, DIN often took the longest to recover.

3.5. Route to Recovery

We can trace the continuous evolution of the system as it warms to, stabilizes at and cools from the 3°C GWL to show the SPG response to forcing (Figure 7). In cumulative emissions phase space, the response in MLD to emissions forcing (Figure 7a) is relatively linear, and the transition to a weakened SPG follows the same trajectory as a transition to a recovered SPG. This is not the case for DIN (Figure 7d) and CHL (Figure 7g). Instead, a non-linear amount of negative emissions forcing is required to recover DIN and CHL back to pre-industrial levels. This non-linear, hysteresis-like response can also been seen for DIN and CHL in both atmospheric pCO_2 and surface air temperature (GMSAT) phase space (Figures 7e, 7f, 7h, and 7i). The response to 3°C GWL zero emissions have also been overlain on Figure 7 (black dots). These clearly show that despite a cessation of emissions and a reduction in atmospheric pCO_2, MLD remains shallow and DIN and CHL continue to decline. This may be associated with continued warming (and hence stronger stratification) which occurs under zero emissions. However, for CHL in surface air temperature phase space in particular (Figure 7i) the hysteresis loop can be closed under negative forcing, which indicates the response to forcing can be fully reversed.

4. Discussion

In summary, our suite of idealized experiments show a decline in MLD, surface dissolved inorganic nitrogen and surface chlorophyll under positive emissions, and the importance of the maximum level of global warming reached in determining how these quantities recover back to pre-industrial levels under zero or negative emissions. When regionally averaged over the SPG, the NAB recovers under zero emissions when the 2°C GWL is not exceeded, but beyond this GWL zero emissions do not lead to recovery. There is significant spatial variation in the recovery trends however, with nutrients and chlorophyll in the Irminger Sea showing a tendency to decline even under negative emissions, while the Labrador Sea showing recovery from even the 5°C GWL.

4.1. A Potential Tipping Threshold Between 2 and 2.5°C GWL

During the positive emissions simulation there is a decline in surface nutrients and chlorophyll, however there is no identified threshold in forcing at which there is a noticeable abrupt decline which is often associated with tipping points. Instead, there is a non-obvious threshold which emerged near 2°C of global warming, defined by the direction of self-sustained system evolution once external forcing (i.e., emissions) cease (see Figure 1a in

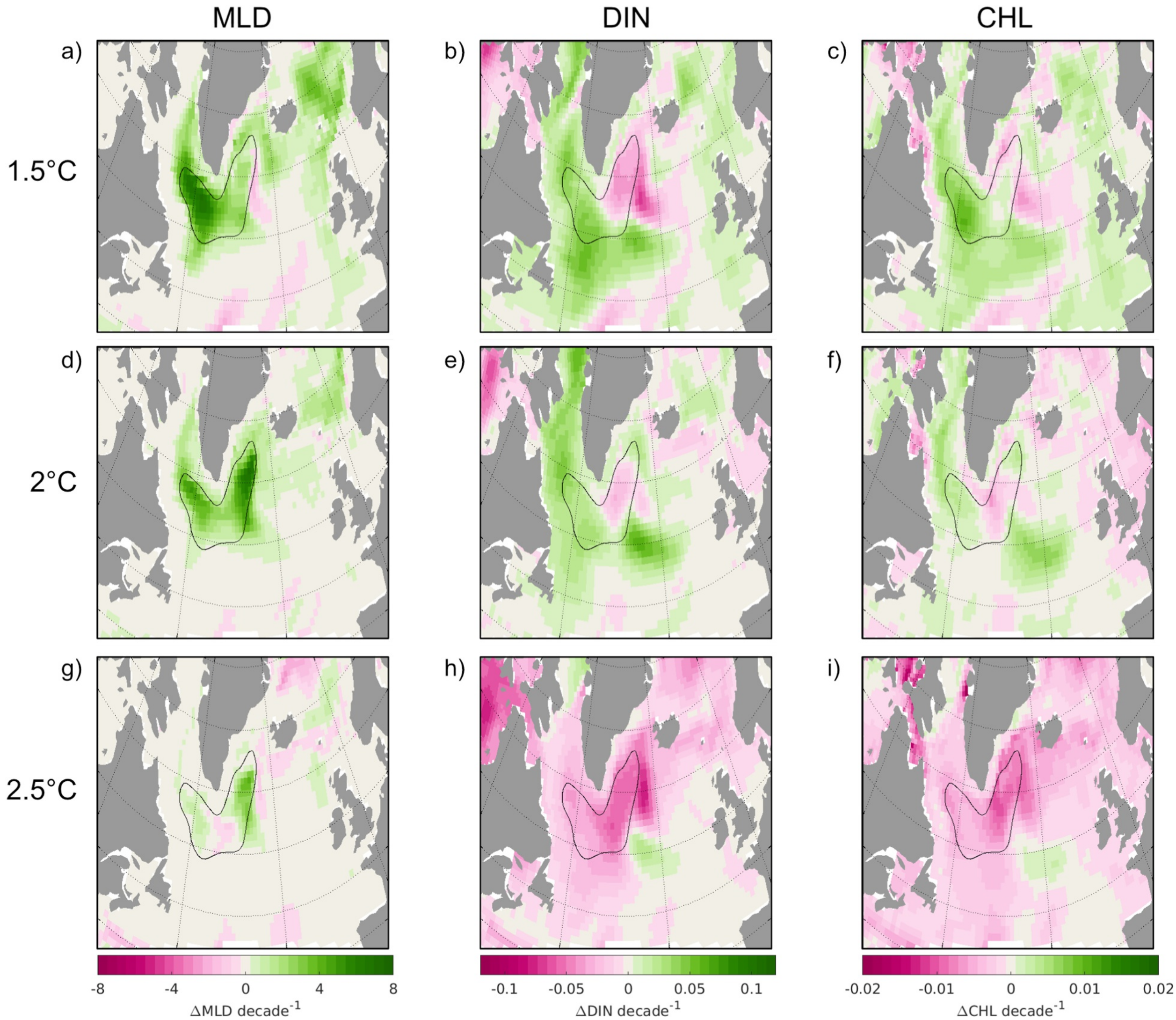

Figure 4. North Atlantic spatial distribution of the mean trend over the (a–c) 1.5°C, (d–f) 2°C and (g–i) 2.5°C Global Warming Level (GWL) zero emissions experiments for (a, d, g) mixed layer depth (MLD) [m per decade], (b, e, h) surface dissolved inorganic nitrogen (DIN) [mmol N m^{-3} per decade] and (c, f, i) surface chlorophyll concentration (CHL) [mg Chl m^{-3} per decade]. The defined subpolar gyre region is overlain (black solid line). The equivalent for the 3°C, 4°C and 5°C GWL zero emissions experiments are shown in Figure S7 in Supporting Information S1.

Feudel, 2023). Below this threshold, once external forcing is stopped the NAB system progresses toward recovery, but above it the NAB continues to decline. Crossing this threshold does not show any noticeable abrupt change in the NAB; instead, it marks a non-apparent transition with no clear early warning, which is arguably worse. This implies that the system can enter a regime in which recovery requires sustained negative emissions, without any obvious signal at the point of crossing.

As self-perpetuating change without external forcing is included in the tipping point definition within the Global Tipping Point Report 2025 (Lenton et al., 2025, p. 48), our results indicate there is a potential tipping threshold for the NAB. More precisely, UKESM has shown that the tipping threshold for the NAB is between 2 and 2.5°C GWL, as zero emissions after 2°C of warming initiates a recovery toward the previous state, while zero emissions after 2.5°C of warming the NAB continues to transition to a different state. To confirm this, the zero emissions simulations would need to be run longer to reach equilibrium and converge upon the new stable state of the NAB. However, these runs are already long enough to understand the long-term direction of self-perpetuating change, and thereby the location of this threshold.

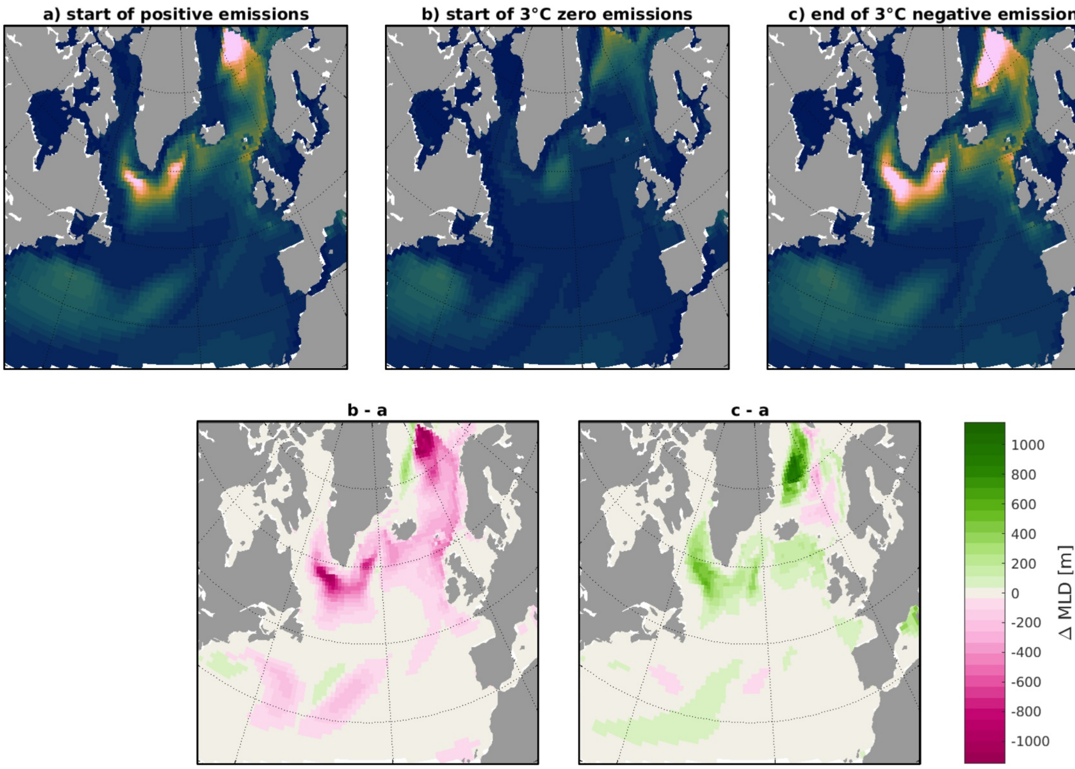

Figure 5. North Atlantic spatial distribution of annual maximum mixed layer depth (MLD) [m] averaged over the (a) first 30 years of the positive emissions, (b) first 30 years of the 3°C zero emissions and (c) final 30 years of the 3°C negative emissions experiments. The change in MLD is shown in the bottom two panels for the (left) b minus a, that is, the change in MLD after positive emissions up to the 3°C Global Warming Level (GWL), and (right) c minus a, that is, the change in MLD after reaching and then returning back down from the 3°C GWL.

4.2. Reversibility

While results show a significant decline in SPG convection and the NAB under positive emissions, we have shown they are potentially reversible, at least when considering regionally averaged surface metrics. Under negative emissions areas of deep convection return in the same regions as before, and regionally averaged surface dissolved inorganic nitrogen and surface chlorophyll return to near pre-industrial levels. However, variables do not return to the exact state they were before; in the following paragraphs we will discuss how (a) MLD overshoots the recovery threshold, (b) the eastern side of the gyre displays less or slower recovery than the western side, and (c) the recovery of the sub-surface nutrients takes longer to recover than the surface.

In the negative emissions experiments which return the cumulative emissions to zero, MLD recovers so much that it overshoots and is deeper than in the pre-industrial. This may be a symptom of the system restabilizing, as has been seen for the Atlantic Meridional Overturning Circulation (AMOC; Cini et al., 2025; van Westen and Dijkstra, 2023). Further, it is possible that MLD might have stabilized back down to pre-industrial MLD had the experiments been run longer and allowed to fully equilibrate under zero cumulative emissions.

Under positive emissions, the decline in surface nutrients and chlorophyll are greater in the Labrador Sea than in the Irminger Sea. While negative emissions subsequently initiate recovery in the Labrador Sea, the Irminger Sea is particularly resilient to reversing the decline. The cause of this difference in both decline and recovery between the regions remains unclear.

While regionally-averaged surface nutrients over the SPG return toward pre-industrial levels, the sub-surface do not, despite negative emissions. Most likely this is because the scenarios have not been run sufficiently long enough to fully reverse the change throughout the deep ocean, which would require timescales on the order of millennia (Wunsch & Heimbach, 2008). This sub-surface nutrient supply may be linked to multiple factors, such as AMOC changes (Boot et al., 2025) and redistribution of nutrients to the deep ocean due to global stratification

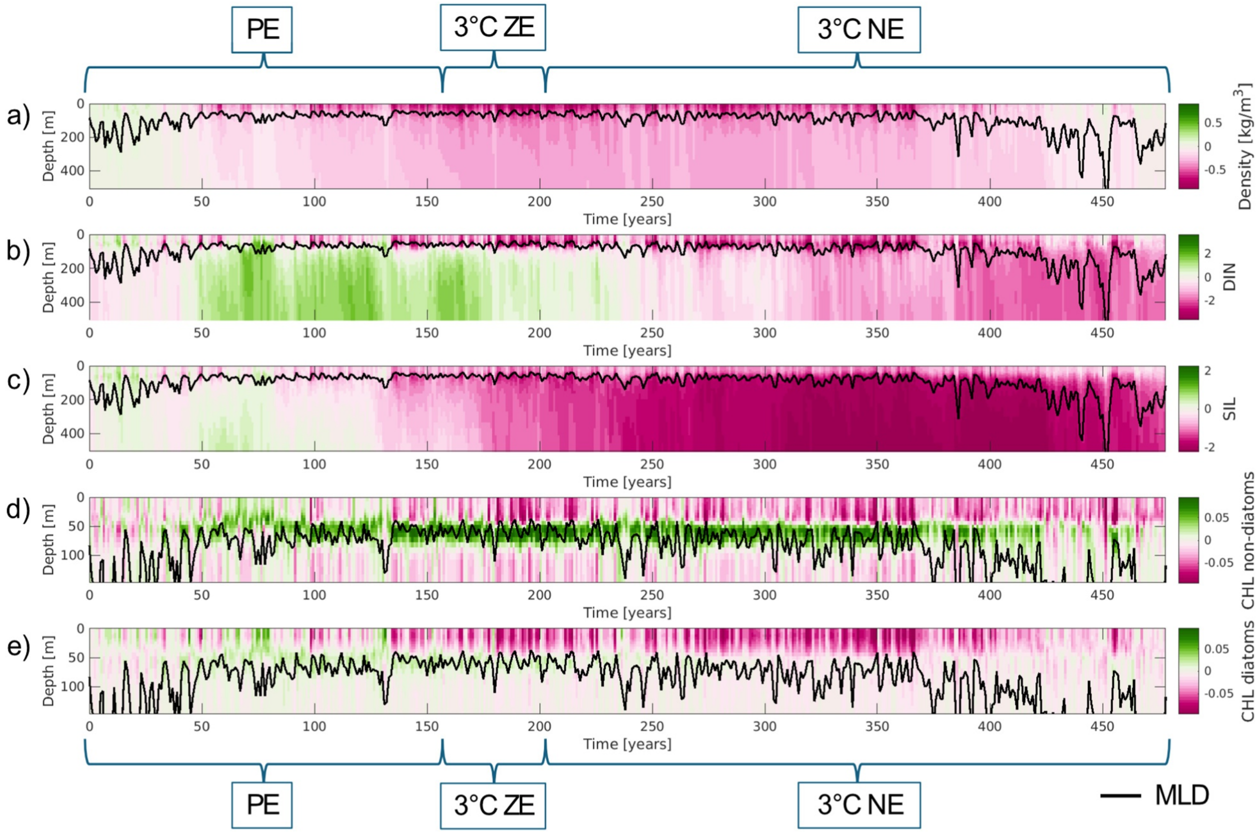

Figure 6. Subpolar gyre regionally averaged water column characteristics through time [years], shown as the difference from the pre-industrial conditions over three different experiments stitched together, encompassing the positive emissions (PE) up to the 3°C Global Warming Level (GWL), the first 50 years of the 3°C GWL zero emissions (ZE), and the 3°C GWL negative emissions (NE) experiments. Shown are the vertical depth profiles of the difference from pre-industrial annual mean (a) density [kg m^{-3}] calculated from temperature and salinity using the SeaWater MATLAB library (Morgan & Pender, 1994), (b) dissolved inorganic nitrogen (DIN) [mmol N m^{-3}], (c) dissolved silicate (SIL) [mmol Si m^{-3}] and chlorophyll (CHL) [mg Chl m^{-3}] of (d) non-diatoms and (e) diatoms. On all subplots absolute annual mean mixed layer depth is overlain as a black line (i.e., not as a difference to the pre-industrial). Note that the pre-industrial water column is taken as an average over the entire pre-industrial simulation. The non-anomaly version of this figure is provided in the supplementary (Figure S14 in Supporting Information S1).

and a sluggish circulation (i.e., nutrient trapping; Liu et al., 2022; Moore et al., 2018). These have long associated timescales and therefore require much longer to fully recover.

4.3. Recovery Timescales

If the 2–2.5°C tipping threshold is not crossed, the earliest extrapolated recovery of the NAB under negative emissions is on the order of centuries, and on the order of millennia under zero emissions. If the 2–2.5°C tipping threshold is surpassed, negative emissions can initiate the recovery of the NAB unless the GWL exceeds 5°C. Again, timescales for this recovery are nearly 500 years (3°C GWL) to many millennia (5°C GWL). These long recovery timescales call into question the practicality of the term "recovery." e.g., a recovery after 100 years would only be seen by human society after 4 generations, and here our findings suggest timescales much longer than this in some cases. This 2–2.5°C tipping threshold could therefore be considered irreversible, at least on human timescales.

Because of the outlier recovery timescales in Table 1, we repeat the above results using an alternative method of trend calculation and find that the extrapolated recovery timescales are highly sensitive to the choice of method. The two methods of trend calculation compared are (a) the mean of the linear regressions over every 30-year segment of the model run (results shown throughout this study and summarized in Table 1), and (b) the linear regression over the whole model run (results shown in Table S2 in Supporting Information S1). We find that with the first method (Table 1), zero emissions initiate recovery for all three metrics when warming does not exceed the 2°C GWL. This indicates a tipping threshold between 2 and 2.5°C, as discussed in Section 4.1. Contrastingly, the

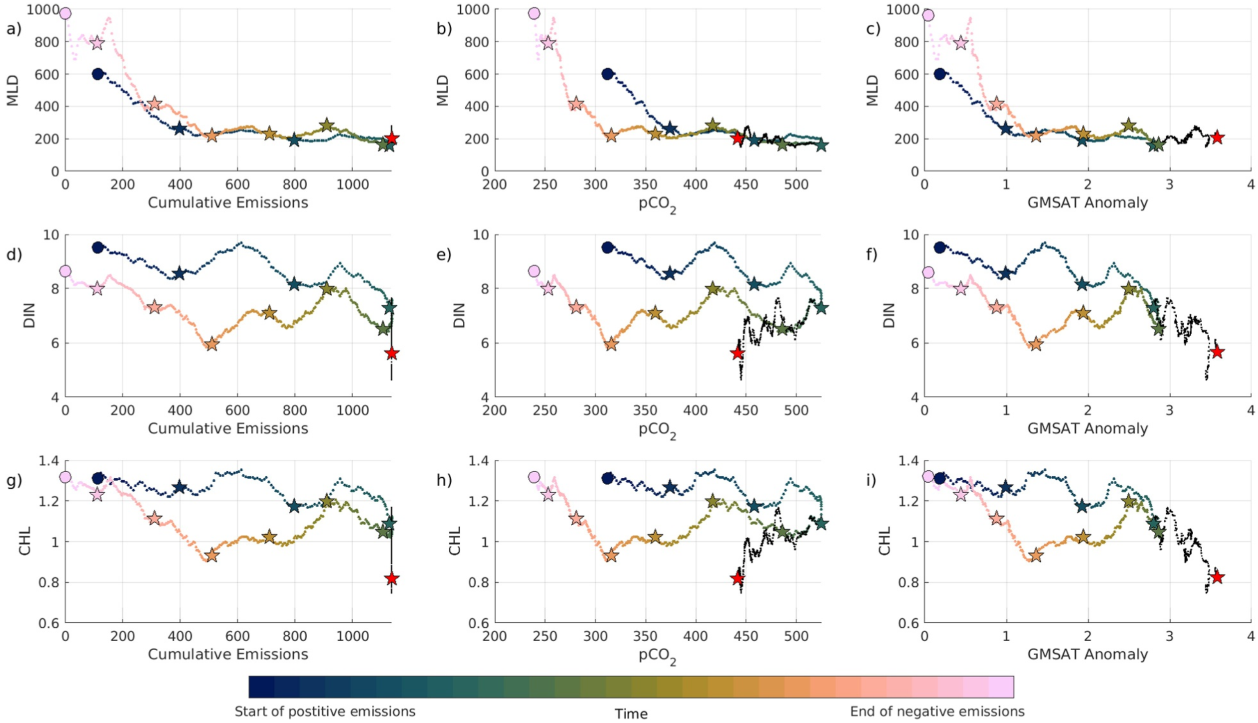

Figure 7. 30-year running mean of subpolar gyre regionally averaged (a–c) mixed layer depth (MLD) [m], (d–f) surface dissolved inorganic nitrogen (DIN) [mmol N m^{-3}] and (g–i) surface chlorophyll (CHL) [mg Chl m^{-3}] plotted against different globally averaged forcing metrics; (a, d, g) cumulative emissions [PgC], (b, e, h) pCO_2 [ppm] and (c, f, i) global mean surface air temperature (GMSAT) anomaly [°C]. The colors depict the time through the scenario which encompasses three different experiments stitched together; the positive emissions up to the 3°C Global Warming Level (GWL), the first 50 years of the 3°C GWL zero emissions, and the 3°C GWL negative emissions, with a colored star every 50 years and the first and last 30-year averages in circles. Note that the 30-year averages are calculated from the 15 years prior to and after each point in time. Black markers are of the full 3°C GWL zero emissions experiment, with the red star for the final 30-year average.

second method yields a tipping threshold between 1.5 and 2°C, as one of the three metrics (surface dissolved inorganic nitrogen) does not recover when zero emissions are applied warmer than the 1.5°C GWL (Table S2 in Supporting Information S1). Therefore, we update the tipping threshold range determined by our study from 2–2.5°C GWL to 1.5–2.5°C GWL.

In some cases, the positive trends in surface dissolved inorganic nitrogen and chlorophyll determined by the first method (Table 1) are so close to zero that the extrapolated recovery time is anomalously large. These anomalies do not appear when using the second method (Table S2 in Supporting Information S1). The example of the 2°C GWL negative emissions experiment is used to compare the two different methods of trend calculation (see Figure S15 in Supporting Information S1), which highlights that the trends and extrapolated recovery timescales are greatly impacted by the method of trend calculation chosen. The uncertainty caused by the need to extrapolate trends to estimate recovery timescales emphasizes the importance of research projects which prioritize long model runs. Note that, as Figure 1 shows (panels d–i), variables (particularly nitrate and chlorophyll) often continue to decline for a period after the end of the positive emissions phase before reversing direction and recovering. As variability is high across all three variables, it is difficult to separate out these periods for our analysis, so we include them within the portions of the time-series used to calculate trends and thereby recovery timescales. The cessation of positive emissions is arguably the most coherent start point for our regressions, so we do not attempt to account for this.

4.4. Model and Experiment Design Caveats

Several important caveats should be noted, both concerning the model UKESM and the experiment design.

Regarding the model itself, the relatively low 1° spatial resolution within UKESM's ocean component means important features such as mesoscale eddies must be parameterized, and therefore changes in mixing processes may be under or overestimated. Although UKESM has previously been run with a 1/4° ocean resolution, it would

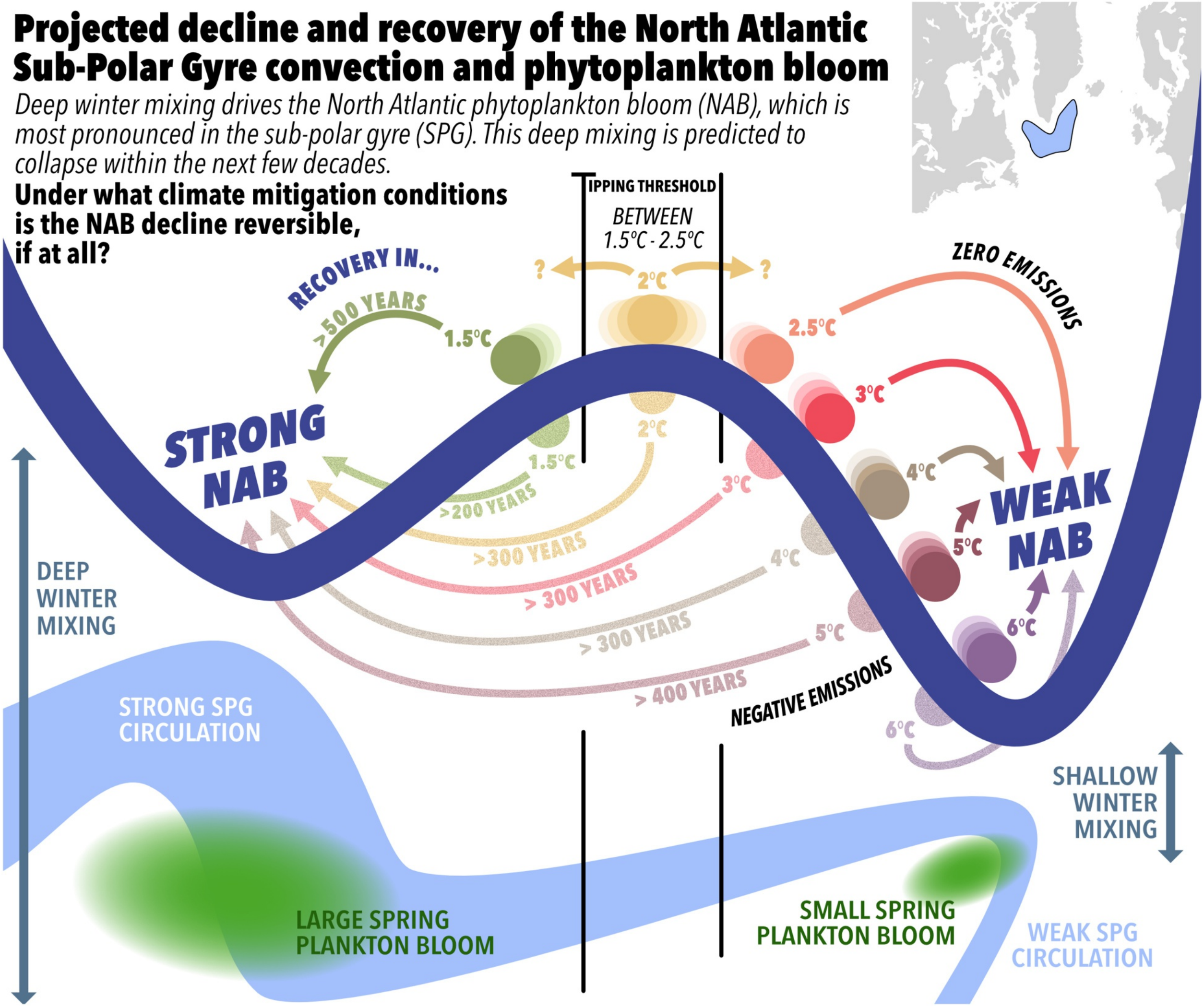

Figure 8. Graphical abstract summarizing the main findings of this study, created by Alexandra Loveridge. The schematic depicts two modes of the biogeochemical state within the North Atlantic subpolar gyre: the left mode with deep winter mixing and a large phytoplankton bloom, and the right mode with shallow mixing and a reduced phytoplankton bloom. The rolling balls represent different scenarios tested in UKESM, such as a 1.5°C globally warmed world, and the arrows indicate the direction in which these scenarios move during zero emissions (above the blue line), and negative emissions (beneath the blue line), that is toward a stronger or weaker bloom state. For the scenarios that track back toward a stronger bloom, recovery timescales are displayed along the arrows. For example, recovery of the bloom after 1.5°C of global warming back to pre-industrial levels took more than 500 years with zero emissions, and more than 200 years with negative emissions. While the 1.5°C scenario tracked toward recovery with zero emissions, the 2.5°C and warmer scenarios continued to decline into a weaker bloom state, and the 2.5°C scenario was unclear as to its direction. This indicated a potential tipping threshold between 1.5 and 2.5°C of global warming, beyond which zero emissions were not sufficient to stop the decline of the North Atlantic phytoplankton bloom.

have been computationally unfeasible to run this suite of experiments at a higher resolution than 1°. The ocean circulation model is therefore too coarse to accurately resolve eddies and boundary currents in the subpolar gyre, which will have consequences for how convection is simulated (e.g., Shan et al., 2024). However, Kelly et al. (2025) found similar abrupt shifts in the subpolar gyre convection in both the 1° and the 1/12° resolution of the ocean circulation model used here, which adds confidence to our results.

Additionally, in this study we use just one ensemble member of one model, which has its own biases (Mulcahy et al., 2023; Sellar et al., 2019; Yool et al., 2021). For example, UKESM has a high climate sensitivity to emissions when compared to other CMIP6 models and therefore will likely have different feedback responses (climate, carbon, etc.) and different SPG and NAB recovery times to the same levels of atmospheric CO_2 and warming examined here.

Regarding the experiment design, these experiments are idealized; the rate of CO_2 addition is constant during the positive emissions phase, and the rate of CO_2 removal from the atmosphere under negative emissions is simply half the rate of addition during positive emissions. The only forcing involved is well-mixed CO_2, and therefore other greenhouse gases and aerosols are not taken into account. Also, the negative emissions experiments vary considerably in their durations and end points. Ideally, this phase would see runs conclude in a standardized manner, and potentially even allow them to persist into a final phase of zero emissions to evaluate "recovery." For various operational reasons (e.g., SPG recovery timescales, available computing resources, staff time for run monitoring) this ideal has not been realized with the result that extrapolation is required, introducing the uncertainty discussed in Section 4.3.

Another caveat is that the defined SPG region over which we regionally average results remains fixed throughout the experiments (see Figure S1 in Supporting Information S1). This region is effectively assumed to encompass the SPG during the different emissions scenarios, an assumption which relies on the SPG to not geographically move or change shape dramatically. We show in Figure S16 in Supporting Information S1 that this assumption generally holds true, as the location and shape of the SSH minimum within the North Atlantic remains relatively consistent when comparing SSH at the start of the positive emissions experiment, start of the 3°C zero emissions experiment, and end of the 3°C negative emissions experiment.

A final caveat to note is that the experiment design does not fully distinguish the impacts on the NAB due to the reduction in SPG deep mixing and due to climate change in general. We can show correlating shifts in both SPG convection and NAB primary productivity, however this does not ensure causation. For example, a decline in NAB productivity may be caused by increasing temperatures instead of due to reduced SPG associated nutrient supply. This, however, is unlikely, as in UKESM productivity rises with temperature. One method to fully attribute NAB decline to a change in the SPG convection would be to include counterfactual runs (Hannart et al., 2016), whereby emissions are increased but the SPG MLD is prevented from shoaling in the model. These runs, when compared to the experiments in which there is a reduction in SPG mixing, would allow the isolation of impacts specifically caused by the SPG convection. However, framing such runs in fully-interactive coupled models can be complicated by the very measures put in place to ensure the counterfactual situations occur (e.g., density-increasing salinity enhancement to counter density-decreasing warming of seawater).

4.5. Policy Implications

Significantly, this work assumes the hypothetical existence of successful, effective and side effect-free carbon dioxide removal technology to achieve its negative emissions. While our results show that significant negative emissions yield the most desirable recovery timescales for the NAB (at least 100 years), the technology to achieve this at an appropriate scale does not currently exist. Nor, for that matter, does the financial or governance infrastructure that would likely be necessary for its successful deployment. Instead, we would stress to policymakers and stakeholders that it is the zero emissions experiments which should be of the greatest interest, rather than the negative emissions.

The main takeaway from this study is that, in the one model tested here, a tipping threshold may lie between 1.5 and 2.5°C of global warming. If crossed, zero emissions cannot stop the decline of the North Atlantic bloom, upon which many ecosystem resources and services depend. Where this threshold lies in other models needs to be tested, therefore initial work is currently underway to carry out a multi-model analysis of North Atlantic biogeochemistry under the same idealized scenarios used here.

It is important to communicate results regarding potential tipping elements clearly, therefore we have provided a graphical abstract summarizing the main findings of this study (Figure 8).The topic of tipping elements can cause confusion and disengagement instead of encouraging and empowering climate action (Kopp et al., 2024). Essentially, by focusing on an extreme system-level change, we may lose sight of the more general degradation leading up to this point, as well as overlook significant regional shifts. The regional impacts of incremental global warming potentially exceed the impact of crossing a tipping threshold. Every degree of warming is therefore equally important to limit even where some key system property—here the North Atlantic phytoplankton bloom—has a specific threshold.

5. Conclusions

- Idealized overshoot experiments allow us to understand how the subpolar gyre (SPG) and North Atlantic phytoplankton bloom (NAB) may respond to future global warming and potential climate mitigation efforts.
- We find under increasing emissions there is a shoaling of mixed layer depth in the subpolar gyre and a decline in surface dissolved inorganic nitrogen and chlorophyll.
- Model results indicate the SPG and NAB will eventually recover back to pre-industrial conditions on, at a minimum, centennial timescales if zero emissions are achieved at a maximum global warming level (GWL) of 1.5–2°C (dependent on the method of trend calculation).
- Zero emissions achieved warmer than 1.5–2°C do not initiate recovery and instead the NAB continues to decline, indicating a tipping threshold between the 1.5 and 2.5°C GWLs.
- Under negative emissions (using negative emissions technology that does not currently exist) SPG convection and the NAB will eventually recover if the GWL does not exceed 5°C, although yet again on centennial recovery timescales.
- Though all experiments in this study are idealized, the zero emissions experiments in particular are intended to help focus climate mitigation efforts and strengthen target goals to limit warming to under the tipping threshold which lies between 1.5 and 2.5°C of mean global warming.
- These results should not overshadow the dominant message to decision makers that every degree of warming is important to limit, nor should the inclusion of negative emissions scenarios overshadow net-zero efforts.

Acknowledgments
The authors are grateful to the referee Amber Boot and the editors for their comments and suggestions which greatly improved the analyses and clarity of this revised paper. We acknowledge support from the UK Natural Environment Research Council under the following projects: (a) TerraFIRMA: Future Impacts, Risks and Mitigation Actions in a changing Earth System project (Grant Reference NE/W004895/1), (b) UKESM: The UK Earth System Modelling Project (Grant Reference NE/N017951/1), and (c) AtlantiS: Atlantic Climate and Environment Impacts (Grant Reference NE/Y005589/1). We acknowledge the project "Exploring Tipping Points and Their Impacts Using Earth System Models", TipESM, funded by the European Union (Grant Agreement number: 101137673; DOI: 10.3030/101137673, Contribution no. 36). This work was funded by UK Research and Innovation (UKRI) under the UK government's Horizon Europe funding Guarantee, with support to U. Reading (Grant Agreement number: 10090271). We acknowledge the project "Optimal High Resolution Earth System Models for Exploring Future Climate Change", OptimESM, funded by the European Union (Grant Agreement number: 101081193). This work was funded by UK Research and Innovation (UKRI) under the UK government's Horizon Europe funding Guarantee, with support to U. Reading (Grant Agreement number: 10040511), Met Office (Grant Agreement number: 10049263) and NOC (Grant Agreement number: 10041076). For both of these projects, the work reflects only the authors' view; the European Commission and their executive agency are not responsible for any use that may be made of the information the work contains. We also acknowledge funding from the project "Progressing Earth System Modelling for Tipping Point Early Warning Systems", PROMOTE (Grant SCOP-PRO1-P027), part of the Forecasting Tipping Points programmer of the Advanced Research + Invention Agency (ARIA). The authors would like to acknowledge use of the CEDA JASMIN computing cluster and British Atmospheric Data Centre data centers in this work, and give additional thanks to the UKESM Core Team for development and maintenance of UKESM, to Till Kuhlbrodt, Steven Rumbold, Jane Mulcahy and Jeremy Walton for generating the model simulations and to Colin Jones for leading the UKESM and TerraFIRMA projects. The authors also want to acknowledge the important role that operational staff from our respective institutes have played in helping do this work.

Conflict of Interest

The authors declare no conflicts of interest relevant to this study.

Availability Statement

All data and code required to repeat the analyses and recreate the results shown in this study can be downloaded from Zenodo (Oliver, 2025).

References

Arellano-Nava, B., Halloran, P. R., Boulton, C. A., Scourse, J., Butler, P. G., Reynolds, D. J., & Lenton, T. M. (2022). Destabilisation of the subpolar North Atlantic prior to the little ice Age. *Nature Communications*, *13*(1), 5008. https://doi.org/10.1038/s41467-022-32653-x

Armstrong McKay, D. I., Staal, A., Abrams, J. F., Winkelmann, R., Sakschewski, B., Loriani, S., et al. (2022). Exceeding 1.5 degrees C global warming could trigger multiple climate tipping points. *Science*, *377*(6611), eabn7950. https://doi.org/10.1126/science.abn7950

Asch, R. G., Stock, C. A., & Sarmiento, J. L. (2019). Climate change impacts on mismatches between phytoplankton blooms and fish spawning phenology. *Global Change Biology*, *25*(8), 2544–2559. https://doi.org/10.1111/gcb.14650

Biri, S., & Klein, B. (2019). North atlantic sub-polar gyre climate index: A new approach. *Journal of Geophysical Research: Oceans*, *124*, 4222–4237. https://doi.org/10.1029/2018JC014822

Boot, A., von der Heydt, A. S., & Dijkstra, H. A. (2023). Effect of Plankton composition shifts in the north Atlantic on atmospheric pCO2. *Geophysical Research Letters*, *50*(2), e2022GL100230. https://doi.org/10.1029/2022gl100230

Boot, A. A., Steenbeek, J., Coll, M., von der Heydt, A. S., & Dijkstra, H. A. (2025). Global marine ecosystem response to a strong AMOC weakening under low and high future emission scenarios. *Earth's Future*, *13*(1), e2024EF004741. https://doi.org/10.1029/2024ef004741

Bopp, L., Aumont, O., Cadule, P., Alvain, S., & Gehlen, M. (2005). Response of diatoms distribution to global warming and potential implications: A global model study. *Geophysical Research Letters*, *32*(19). https://doi.org/10.1029/2005gl023653

Born, A., Mignot, J., & Stocker, T. F. (2015). Multiple equilibria as a possible mechanism for decadal variability in the North Atlantic Ocean. *Journal of Climate*, *28*, 8907–8922. https://doi.org/10.1175/jcli-d-14-00813.1

Brovkin, V., Brook, E., Williams, J. W., Bathiany, S., Lenton, T. M., Barton, M., et al. (2021). Past abrupt changes, tipping points and cascading impacts in the Earth system. *Nature Geoscience*, *14*(8), 550–558. https://doi.org/10.1038/s41561-021-00790-5

Cabrera-Brufau, M., Arin, L., Sala, M. M., Cermeño, P., & Marrasé, C. (2021). Diatom dominance enhances resistance of phytoplanktonic POM to mesopelagic microbial decomposition. *Frontiers in Marine Science*, *8*, 683354. https://doi.org/10.3389/fmars.2021.683354

Cini, M., Zappa, G., Ragone, F., & Corti, S. (2025). Noise-shaped hysteresis cycles of the AMOC under increasing CO2 forcing. *Chaos: An Interdisciplinary Journal of Nonlinear Science*, *35*(2), 023167. https://doi.org/10.1063/5.0241503

CMEMS. (2023). E.U. copernicus marine service information. In *Global Ocean Colour (Copernicus-GlobColour), Bio-Geo-Chemical, L4 (monthly and interpolated) from Satellite Observations (1997-ongoing)*. Marine Data Store (MDS). https://doi.org/10.48670/moi-00281

de Boyer Montégut, C. (2023). *Mixed layer depth climatology computed with a density threshold criterion of 0.03kg/m3 from 10 m depth value*. SEANOE. https://doi.org/10.17882/91774

de Boyer Montégut, C., Madec, G., Fischer, A. S., Lazar, A., & Daniele, I. (2004). Mixed layer depth over the global ocean: An examination of profile data and a profile-based climatology. *Journal of Geophysical Research*, *109*(C12). https://doi.org/10.1029/2004jc002378

Feudel, U. (2023). Rate-induced tipping in ecosystems and climate: The role of unstable states, basin boundaries and transient dynamics. *Nonlinear Processes in Geophysics*, *30*(4), 481–502. https://doi.org/10.5194/npg-30-481-2023

Foukal, N. P., & Lozier, M. S. (2017). Assessing variability in the size and strength of the North Atlantic subpolar gyre. *Journal of Geophysical Research: Oceans*, *122*(8), 6295–6308. https://doi.org/10.1002/2017jc012798

Fu, W., Randerson, J. T., & Keith Moore, J. (2016). Climate change impacts on net primary production (NPP) and export production (EP) regulated by increasing stratification and phytoplankton community structure in the CMIP5 models. *Biogeosciences*, *13*(18), 5151–5170. https://doi.org/10.5194/bg-13-5151-2016

Garcia, H. E., Weathers, K., Paver, C. R., Smolyar, I., Boyer, T. P., Locarnini, R. A., et al. (2018). In A. Mishonov Technical (Ed.), *World Ocean Atlas 2018, volume 4: Dissolved Inorganic Nutrients (phosphate, nitrate and nitrate+nitrite, silicate)*. NOAA Atlas NESDIS 84.

Gohin, F., Druon, J. N., & Lampert, L. (2010). A five channel chlorophyll concentration algorithm applied to SeaWiFS data processed by SeaDAS in coastal waters. *International Journal of Remote Sensing*, *23*(8), 1639–1661. https://doi.org/10.1080/01431160110071879

Grieve, B. D., Hare, J. A., & Saba, V. S. (2017). Projecting the effects of climate change on Calanus finmarchicus distribution within the U.S. Northeast Continental Shelf. *Scientific Reports*, *7*(1), 6264. https://doi.org/10.1038/s41598-017-06524-1

Gu, Q., Gervais, M., Danabasoglu, G., Kim, W. M., Castruccio, F., Maroon, E., & Xie, S. P. (2024). Wide range of possible trajectories of North Atlantic climate in a warming world. *Nature Communications*, *15*(1), 4221. https://doi.org/10.1038/s41467-024-48401-2

Hannart, A., Pearl, J., Otto, F. E. L., Naveau, P., & Ghil, M. (2016). Causal counterfactual theory for the attribution of weather and climate-related events. *Bulletin of the American Meteorological Society*, *97*(1), 99–110. https://doi.org/10.1175/bams-d-14-00034.1

Henson, S., Cole, H., Beaulieu, C., & Yool, A. (2013). The impact of global warming on seasonality of ocean primary production. *Biogeosciences*, *10*(6), 4357–4369. https://doi.org/10.5194/bg-10-4357-2013

Henson, S. A., Cole, H. S., Hopkins, J., Martin, A. P., & Yool, A. (2017). Detection of climate change-driven trends in phytoplankton phenology. *Global Change Biology*, *24*(1), e101–e111. https://doi.org/10.1111/gcb.13886

Henson, S. A., John, P. D., & Sarmiento, J. L. (2009). Decadal variability in North Atlantic phytoplankton blooms. *Journal of Geophysical Research*, *114*, C04013. https://doi.org/10.1029/2008JC005139

Hieronymus, J., Hieronymus, M., Gröger, M., Schwinger, J., Bernadello, R., Tourigny, E., et al. (2024). Net primary production annual maxima in the North Atlantic projected to shift in the 21st century. *Biogeosciences*, *21*(9), 2189–2206. https://doi.org/10.5194/bg-21-2189-2024

Jacobsen, S., Gaard, E., & Hátún, H. (2022). Declining pre-bloom Calanus finmarchicus egg production adjacent to two major overwintering regions in the Northeastern Atlantic. *Frontiers in Marine Science*, *9*, 822978. https://doi.org/10.3389/fmars.2022.822978

Jalali, B., Sicre, M.-A., Azuara, J., Pellichero, V., & Combourieu-Nebout, N. (2019). Influence of the North Atlantic subpolar gyre circulation on the 4.2 ka BP event. *Climate of the Past*, *15*(2), 701–711. https://doi.org/10.5194/cp-15-701-2019

Jensen, L. Ø., Mousing, E. A., & Richardson, K. (2017). Using species distribution modelling to predict future distributions of phytoplankton: Case study using species important for the biological pump. *Marine Ecology*, *38*(3), e12427. https://doi.org/10.1111/maec.12427

Kelly, S., Popova, E., Yool, A., Jebri, F., Oliver, S., & Srokosz, M. (2025). Abrupt changes in the timing and magnitude of the north Atlantic bloom over the 21st century. *Journal of Geophysical Research: Oceans*, *130*(3), e2024JC022284. https://doi.org/10.1029/2024jc022284

Klus, A., Prange, M., Varma, V., Tremblay, L. B., & Schulz, M. (2018). Abrupt cold events in the North Atlantic Ocean in a transient Holocene simulation. *Climate of the Past*, *14*(8), 1165–1178. https://doi.org/10.5194/cp-14-1165-2018

Kopp, R. E., Gilmore, E. A., Shwom, R. L., Adams, H., Adler, C., Oppenheimer, M., et al. (2024). Tipping points' confuse and can distract from urgent climate action. *Nature Climate Change*, *15*(1), 29–36. https://doi.org/10.1038/s41558-024-02196-8

Kuhlbrodt, T., Jones, C. G., Sellar, A., Storkey, D., Blockley, E., Stringer, M., et al. (2018). The low-resolution version of HadGEM3 GC3.1: Development and evaluation for global climate. *Journal of Advances in Modeling Earth Systems*, *10*(11), 2865–2888. https://doi.org/10.1029/2018ms001370

Kwiatkowski, L., Torres, O., Bopp, L., Aumont, O., Chamberlain, M., Christian, J. R., et al. (2020). Twenty-first century ocean warming, acidification, deoxygenation, and upper-ocean nutrient and primary production decline from CMIP6 model projections. *Biogeosciences*, *17*(13), 3439–3470. https://doi.org/10.5194/bg-17-3439-2020

Lavoie, D., Lambert, N., & Gilbert, D. (2017). Projections of future trends in biogeochemical conditions in the Northwest Atlantic using CMIP5 Earth System models. *Atmosphere-Ocean*, *57*(1), 18–40. https://doi.org/10.1080/07055900.2017.1401973

Lenton, T. M., Milkoreit, M., Willcock, S., Abrams, J. F., Armstrong McKay, D. I., Buxton, J. E., et al. (2025). *The global tipping points report*. University of Exeter.

Liu, Y., Moore, J. K., Primeau, F., & Wang, W. L. (2022). Reduced CO2 uptake and growing nutrient sequestration from slowing overturning circulation. *Nature Climate Change*, *13*(1), 83–90. https://doi.org/10.1038/s41558-022-01555-7

Madec, G., Bell, M., Blaker, A., Bricaud, C., Bruciaferri, D., Castrillo, M., et al. (2023). *NEMO Ocean engine reference manual*. Zenodo.

Mayor, D. J., Cook, K. B., Anderson, T. R., Belcher, A., Jenkins, H., Lindeque, P., et al. (2020). Marine copepods, the wildebeest of the Ocean. *Frontiers for Young Minds*, *8*, 18. https://doi.org/10.3389/frym.2020.00018

Menary, M. B., Jackson, L. C., Wood, R. A., & Betts, R. A. (2025). Abrupt changes in the subpolar North Atlantic and their impact on the climate of the British isles. *Geophysical Research Letters*, *52*(9), e2024GL113871. https://doi.org/10.1029/2024gl113871

Moore, J. K., Fu, W., Primeau, F., Gregory Britten, L., Lindsay, K., Long, M., et al. (2018). Sustained climate warming drives declining marine biological productivity. *Science*, *359*(6380), 1139–1143. https://doi.org/10.1126/science.aao6379

Morgan, P. P., & Pender, L. (1994). *The SeaWater MATLAB library for calculating the EOS-80 properties of sea water*. CSIRO Marine Research. Release 1.2d.

Moyano, M., Illing, B., Akimova, A., Alter, K., Bartolino, V., Börner, G., et al. (2022). Caught in the middle: Bottom-up and top-down processes impacting recruitment in a small pelagic fish. *Reviews in Fish Biology and Fisheries*. https://doi.org/10.1007/s11160-022-09739-2

Mulcahy, J. P., Jones, C. G., Rumbold, S. T., Kuhlbrodt, T., Dittus, A. J., Blockley, E. W., et al. (2023). UKESM1.1: Development and evaluation of an updated configuration of the UK Earth System Model. *Geoscientific Model Development*, *16*(6), 1569–1600. https://doi.org/10.5194/gmd-16-1569-2023

Nakamura, Y., & Oka, A. (2019). CMIP5 model analysis of future changes in ocean net primary production focusing on differences among individual oceans and models. *Journal of Oceanography*, *75*(5), 441–462. https://doi.org/10.1007/s10872-019-00513-w

Oliver, S. (2025). Data supplement for Oliver et al. "The North Atlantic sub-polar gyre and phytoplankton bloom under potential future climate scenarios" (Version 1) [Dataset]. *Zenodo*. https://doi.org/10.5281/zenodo.16992761

Pawlowicz, R. (2005). M_Map: A mapping package for MATLAB, version 1.4c [Computer software]. available online at www.eoas.ubc.ca/~rich/map.html

Pershing, A. J., & Stamieszkin, K. (2020). The north Atlantic ecosystem, from Plankton to whales. *Annual Review of Marine Science*, *12*(1), 339–359. https://doi.org/10.1146/annurev-marine-010419-010752

Ridley, J. K., Blockley, E. W., Keen, A. B., Rae, J. G. L., West, A. E., & Schroeder, D. (2018). The sea ice model component of HadGEM3-GC3.1. *Geoscientific Model Development*, *11*(2), 713–723. https://doi.org/10.5194/gmd-11-713-2018

Sein, D. V., Gröger, M., Cabos, W., Alvarez-Garcia, F. J., Mikolajewicz, U., Hagemann, S., et al. (2020). Regionally coupled Atmosphere-Ocean-Marine Biogeochemistry model ROM: 2. Studying the climate change signal in the North Atlantic and Europe. *Journal of Advances in Modeling Earth Systems*, *12*(8), e2019MS001646. https://doi.org/10.1029/2019ms001646

Sellar, A. A., Jones, C. G., Mulcahy, J. P., Tang, Y., Yool, A., Wiltshire, A., et al. (2019). UKESM1: Description and evaluation of the U.K. Earth System model. *Journal of Advances in Modeling Earth Systems*, *11*(12), 4513–4558. https://doi.org/10.1029/2019ms001739

Sgubin, G., Swingedouw, D., Drijfhout, S., Mary, Y., & Bennabi, A. (2017). Abrupt cooling over the North Atlantic in modern climate models. *Nature Communications*, *8*(1), 14375. https://doi.org/10.1038/ncomms14375

Shan, X., Sun, S., Wu, L., & Spall, M. (2024). Role of the Labrador Current in the Atlantic Meridional Overturning Circulation response to greenhouse warming. *Nature Communications*, *15*(1), 7361. https://doi.org/10.1038/s41467-024-51449-9

Smith, R. S., Bilge, T. A., Bracegirdle, T. J., Holland, P. R., Kuhlbrodt, T., Lang, C., et al. (2026). Response of ice sheets, sea-ice and sea level in climate stabilisation and reversibility simulations using a state-of-the-art Earth System Model. *Earth System Dynamics*, *17*(3), 475–493. https://doi.org/10.5194/esd-17-475-2026

Smith, R. S., Mathiot, P., Siahaan, A., Lee, V., Cornford, S. L., Gregory, J. M., et al. (2021). Coupling the U.K. Earth System model to dynamic models of the Greenland and antarctic ice sheets. *Journal of Advances in Modeling Earth Systems*, *13*(10), e2021MS002520. https://doi.org/10.1029/2021ms002520

Storkey, D., Blaker, A. T., Mathiot, P., Megann, A., Aksenov, Y., Blockley, E. W., et al. (2018). UK Global Ocean GO6 and GO7: A traceable hierarchy of model resolutions. *Geoscientific Model Development*, *11*(8), 3187–3213. https://doi.org/10.5194/gmd-11-3187-2018

Swingedouw, D., Bily, A., Esquerdo, C., Borchert, L. F., Sgubin, G., Mignot, J., & Menary, M. (2021). On the risk of abrupt changes in the North Atlantic subpolar gyre in CMIP6 models. *Annals of the New York Academy of Sciences*, *1504*(1), 187–201. https://doi.org/10.1111/nyas.14659

Swingedouw, D., Speranza, C. I., Bartsch, A., Durand, G., Jamet, C., Beaugrand, G., & Conversi, A. (2020). Early warning from space for a few key tipping points in physical, biological, and social-ecological systems. *Surveys in Geophysics*, *41*(6), 1237–1284. https://doi.org/10.1007/s10712-020-09604-6

Terpstra, S., Falkena, S. K. J., Bastiaansen, R., Bathiany, S., Dijkstra, H. A., & von der Heydt, A. S. (2025). Assessment of abrupt shifts in CMIP6 models using edge detection. *AGU Advances*, *6*(3), e2025AV001698. https://doi.org/10.1029/2025av001698

Thomas, Z. A. (2016). Using natural archives to detect climate and environmental tipping points in the Earth System. *Quaternary Science Reviews*, *152*, 60–71. https://doi.org/10.1016/j.quascirev.2016.09.026

Tollefson, J. (2025). Earth breaches 1.5° C climate limit for the first time: What does it mean? *Nature*, *637*(8047), 769–770. https://doi.org/10.1038/d41586-025-00010-9

van Westen, R. M., & Dijkstra, H. A. (2023). Asymmetry of AMOC hysteresis in a State-Of-The-Art global climate model. *Geophysical Research Letters*, *50*. https://doi.org/10.1029/2023GL106088

Williams, K. D., Copsey, D., Blockley, E. W., Bodas-Salcedo, A., Calvert, D., Comer, R., et al. (2018). The Met Office Global Coupled Model 3.0 and 3.1 (GC3.0 and GC3.1) configurations. *Journal of Advances in Modeling Earth Systems*, *10*(2), 357–380. https://doi.org/10.1002/2017ms001115

Winkelmann, R., Dennis, D. P., Donges, J. F., Loriani, S., Klose, A. K., Abrams, J. F., et al. (2025). The Tipping Points Modelling Intercomparison Project (TIPMIP): Assessing tipping point risks in the Earth system [preprint]. *EGUsphere*. https://egusphere.copernicus.org/preprints/2025/egusphere-2025-1899/

Wunsch, C., & Heimbach, P. (2008). How long to oceanic tracer and proxy equilibrium? *Quaternary Science Reviews*, *27*(7–8), 637–651. https://doi.org/10.1016/j.quascirev.2008.01.006

Wyser, K., Kjellström, E., Koenigk, T., Martins, H., & Döscher, R. (2020). Warmer climate projections in EC-Earth3-Veg: The role of changes in the greenhouse gas concentrations from CMIP5 to CMIP6. *Environmental Research Letters*, *15*(5), 054020. https://doi.org/10.1088/1748-9326/ab81c2

Yamaguchi, R., Rodgers, K. B., Timmermann, A., Stein, K., Sarah, S., Bianchi, D., et al. (2022). Trophic level decoupling drives future changes in phytoplankton bloom phenology. *Nature Climate Change*, *12*(5), 469–476. https://doi.org/10.1038/s41558-022-01353-1

Yool, A., Palmiéri, J., Jones, C. G., de Mora, L., Kuhlbrodt, T., Popova, E. E., et al. (2021). Evaluating the physical and biogeochemical state of the global ocean component of UKESM1 in CMIP6 historical simulations. *Geoscientific Model Development*, *14*(6), 3437–3472. https://doi.org/10.5194/gmd-14-3437-2021

Yool, A., Popova, E. E., & Anderson, T. R. (2013). MEDUSA-2.0: An intermediate complexity biogeochemical model of the marine carbon cycle for climate change and ocean acidification studies. *Geoscientific Model Development*, *6*(5), 1767–1811. https://doi.org/10.5194/gmd-6-1767-2013

Yool, A., Popova, E. E., & Coward, A. C. (2015). Future change in ocean productivity: Is the Arctic the new Atlantic? *Journal of Geophysical Research: Oceans*, *120*(12), 7771–7790. https://doi.org/10.1002/2015jc011167